

## CHANDRA OBSERVATION OF LMXBS IN THE ELLIPTICAL GALAXY M84

A. FINOGENOV<sup>1,2</sup>, AND C. JONES<sup>2</sup>

<sup>1</sup> Max-Planck-Institut für extraterrestrische Physik, Giessenbachstraße, 85748 Garching, Germany

<sup>2</sup> Smithsonian Astrophysical Observatory, 60 Garden st., MS 3, Cambridge, MA 02138, USA

*submitted to ApJ, June 28 2001; accepted April 2 2002*

### ABSTRACT

We present characteristics of the X-ray point source population in the M84 galaxy, observed by *Chandra* ACIS-S. We find an excess in the number of sources centered on M84, with a spatial distribution closely corresponding to the M84 stellar light. Given an absence of recent star-formation, accreting binaries are the only candidates for the M84 X-ray sources. The majority of M84 sources (with luminosities exceeding  $10^{38}$  ergs/s) exhibit hardness ratios expected from multi-temperature black-body disk emission. The most luminous sources, which we attribute to accreting black holes exhibit X-ray colors typical of a black body spectrum. We also identify the sources whose X-ray colors match the expectations for constituents of the Cosmic X-ray Background. The number of such sources agrees with that expected to be background sources. After correcting for incompleteness in the source detection, we find a  $\log(N) - \log(S)$  for M84 similar to that of the elliptical galaxy NGC4697, i.e. having a break at a luminosity of  $L_b = 2.4_{-0.3}^{+0.6} \times 10^{38}$  ergs/s, approximately the Eddington limit on the isotropic luminosity for accretion onto a neutron star. The slope of the luminosity function above the break provides evidence for a mass distribution in the M84 accreting black holes.

*Subject headings:* Galaxies: elliptical and lenticular — galaxies individual: NGC4374 (M84) — X-Rays: galaxies — Stars: binaries: close — X-Rays: stars

### 1. INTRODUCTION

Observation of X-ray sources in the Milky Way galaxy began with the launch of the first X-ray detector (Giacconi et al. 1962). The study of accreting systems at all wavelengths is now a well-developed field (for a recent review see Tanaka & Shibazaki 1996; theoretical progress is presented by Iben et al. 1995; Kalogera & Webbink 1998). With the advent of high angular resolution X-ray observations, first with Einstein and ROSAT and now with Chandra and XMM-Newton, it has become feasible to study the X-ray populations in other galaxies.

This *Paper* presents a detailed study of Chandra observation of the point sources in M84, an elliptical galaxy in the core of the Virgo cluster (study of the diffuse X-ray emission of M84 is presented in Finoguenov & Jones 2001). The particular importance of population studies in early-type galaxies comes from the small number of possible avenues leading to the X-ray source production. As most ellipticals are old stellar systems, only accretion of matter in low mass X-ray binaries (LMXB) can provide enough power to explain X-ray luminosities that exceed  $10^{37}$  ergs/s. The question of how low is the mass of the secondary star is closely connected to studies of the stellar population (*e.g.* Worthey 1994) and recent merger activity (*e.g.* Schweizer & Seizer 1992). The latter can be responsible for differences in the X-ray population in the centers of galaxies, compared to that in the halos. The dependence of LMXB activity on star-formation rate is considered in White & Ghosh (1998).

When one star in a binary system becomes a compact object (primary), the accretion process can be triggered through the Roche-lobe overflow of material from the evolved low-mass companion star (secondary). Another mechanism for triggering accretion at epochs long

after the cessation of star-formation, is by shrinking the binary star separation through magnetic braking (outward transport of the angular momentum in magnetic stellar winds, Verbunt & Zwaan 1981) or gravitational radiation losses (Paczynski 1967) leading to accretion even from a main sequence star. Accretion onto a white dwarf is identified through a super-soft X-ray spectrum (*e.g.* Kahabka & van der Heuvel 1997). However, our observation is not sensitive to this mechanism, since detecting white dwarfs in our softest energy band (0.3 – 1 keV) would imply a luminosity for the source (calculated assuming a spectral temperature of 35 eV), far exceeding the corresponding Eddington limit.

The luminosity function of X-ray sources in M84 can be expressed as a convolution of the accreting binary mass-function and X-ray luminosity function for equal mass primaries. Neutron stars, the most numerous class of accreting binary primaries, have very similar masses,  $1.4 M_{\odot}$ . Thus, the source luminosity function below the Eddington luminosity for a neutron star ( $1.8 \times 10^{38}$  ergs/s) is dominated by the X-ray luminosity function of neutron-star LMXB (NS LMXB). Their luminosities are proportional to the accretion rate determined by the orbital period and mass loss (Wu 2001). Most of the known black-holes in binary systems have a mass of  $6 M_{\odot}$  (Tanaka & Shibazaki 1996), however recent studies indicate a more complicated black hole mass function (Bailyn et al. 1998; Fryer & Kalogera 2001).

In this *Paper* we study the spatial distribution of LMXB in M84 (§3) and derive the integral  $\log(N) - \log(S)$  distribution (§4). We study source hardness ratios and conclude with a discussion on the emission mechanism for LMXB (§5). Interpretation of the M84 LMXB luminosity function is given in §6.

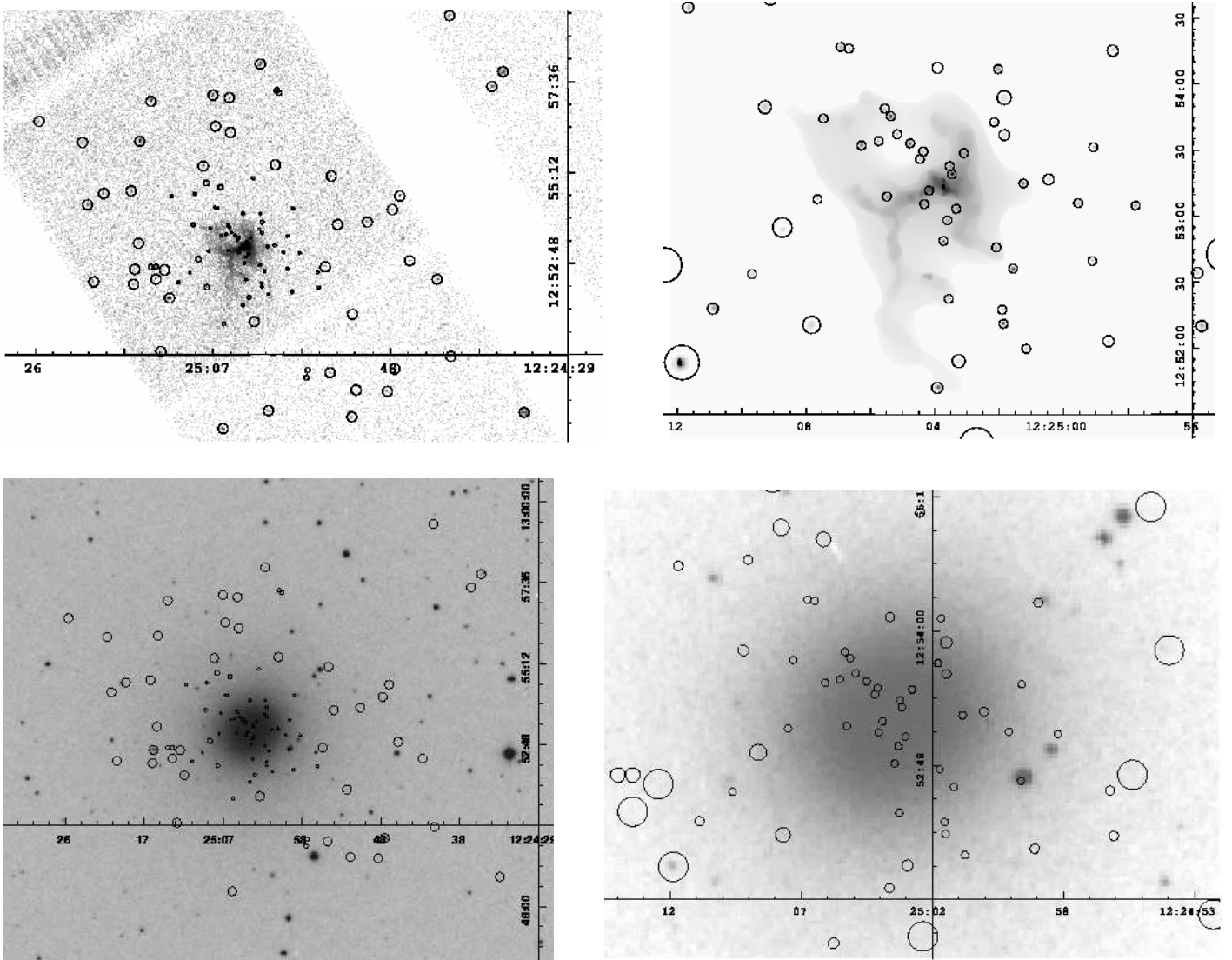


FIG. 1.— *Upper panels:* Chandra image of the ACIS field around M84 (*left*) and wavelet-decomposed image of the central part of M84 (*right*), used to calculate the source surface density. Circles mark individual point sources. The energy band is 0.4–5.0 keV. *Lower row:* DSS (optical) image of M84 overlaid with X-ray point source positions.

## 2. ANALYSIS OF THE ACIS OBSERVATION

In the ACIS-S 28.7 ksec observation of M84, point source detection was done in the 0.4–5.0 keV energy band, where the source signal-to-noise is highest. Throughout sections §3–§5, luminosities are cited for the 0.4–10 keV band, using the countrate-to-luminosity conversion for the best-fit power law photon index of 1.4, derived for the combined spectra of all point sources within two effective radii (Finoguenov & Jones 2001). Given the duration of the observation, and assuming a 17 Mpc distance to M84, one ACIS-S count corresponds to  $10^{37}$  ergs/s. Estimates of the detection rate for the background sources were made using a power law photon index  $\Gamma = 1.7$  and the  $\log(N) - \log(S)$  determination by Giacconi et al. (2001).

Source detection was carried out using the matched filter (wavelet) technique (Vikhlinin et al. 1995). We performed simulations to estimate the detection efficiency of this method on our field, as described below (§4). In addition we estimate the effects of variations in the PSF on the resulting signal-to-noise and thus source detection efficiency. Variations in the PSF cause the apparent source size to increase with increasing off-axis angle. Thus, we run the detection procedure twice, first for the central  $10'$  radius region, where we use a full resolution ACIS pixel image ( $0.492''$  on a side) and second employing a 4 by 4 pixel binning for the full  $15.6' \times 11.1'$  field, shown in Fig.1, which includes S3 and portions of S2, I2 and I3 chips. At large radii, a decrease in the detection efficiency arises due to the larger detection region for the source counts and therefore for the background. We merged the source lists from the two methods, thus removing duplications. To determine the source count rate, we calculate exposure maps, accounting for the spatial non-uniformity of the CCD quantum efficiency. We take vignetting (weighted by the mean spectrum of sources,  $\Gamma = 1.4$ ) and dithering into account, using CIAO contributed software.

## 3. SPATIAL DISTRIBUTION OF X-RAY BINARIES IN M84

Before we proceed to describe our results, we note that for M84, we can study the X-ray population at a few effective radii, while strong diffuse emission prevents us from detecting faint sources very close to the galaxy center.

The Chandra ACIS image of the M84 field is shown in Fig.1. We show X-ray images of the full field and the center of M84 with detected sources marked with circles. The enhanced background (in the upper left of the top left image) is from a neighboring CCD chip (S4), which we omitted from analysis.

Of the 106 sources shown in Fig.1 we exclude 3 sources associated with foreground objects from all subsequent analysis. We identified these as corresponding to an optical counterpart of size or luminosity exceeding that expected for globular clusters at the M84 distance. Spatial analysis of the source density does not reveal any peculiarities at the  $5\sigma$  level. At the  $3\sigma$  significance level (Fig.2), a clustering of sources on sub-arcminute angular scale is seen, as well as the effect of non-uniform source detection in regions with strong diffuse emission, corresponding to the  $\mathcal{H}$ -shape of the hot gas in M84, seen in the upper panels of Fig.1. Strong clustering on sub-arcminute angular scales is an attribute of the sources that constitute the Cosmic X-ray Background (*e.g.* Vikhlinin & Forman

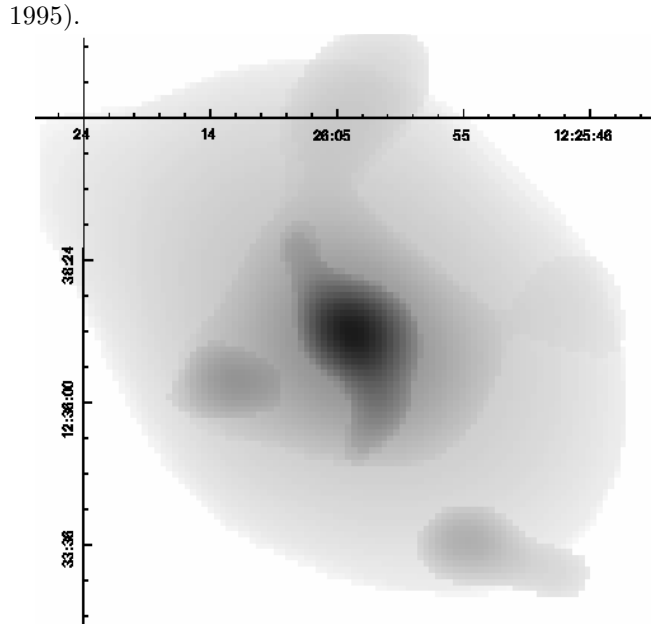


FIG. 2.— Map of the surface source number density in M84. The major concentration of sources is due to LMXBs following the light of the galaxy and is centered on M84. Deviations from the symmetry around the center are caused by variation in the detection threshold due to strong diffuse emission as well as contributions from the CXB sources, which exhibit pronounced source clustering on sub-arcminute angular scales.

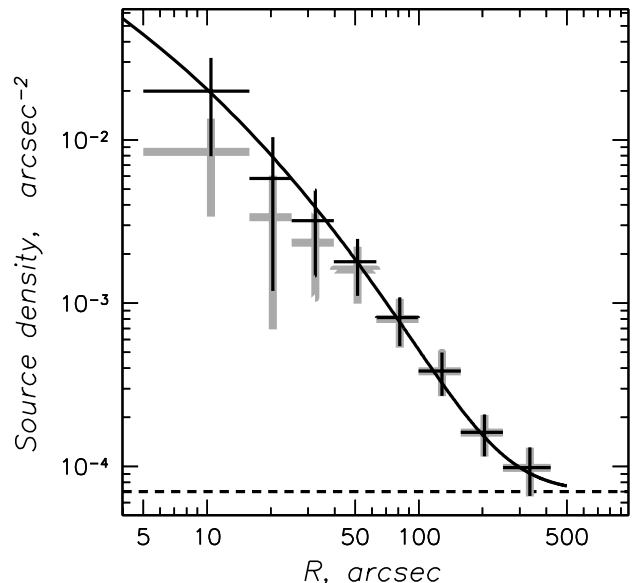


FIG. 3.— Source number density profile. The solid line denotes the galaxy light profile. The black (grey) crosses denote the distribution of Chandra sources corrected (uncorrected) for reduced detection efficiency due to the presence of the diffuse source. A dashed line shows the expected level of background X-ray sources (Giacconi et al. 2001).

The profile of the source number density, centered on M84, is presented in Fig.3. While the outer part is described well by the stellar light distribution, taken as a de Vaucouleurs (1/4) law with  $r_e = 1'$  (where  $r_e$  is the effective radius, within which the galaxy contains half of its light), the center reveals a deficit of sources, due to the high detection threshold, caused by the bright diffuse X-ray emission. In the next section, we develop a method to correct for this effect, with the results also shown in Fig.3.

With the normalization shown in Fig.3, and assuming

a distance to M84 of 17 Mpc (the corresponding luminosity in the B band is  $L_B = 4.5 \times 10^{10} L_\odot$  within  $r_e$ ), the LMXB rate per  $L_B/10^{10} L_\odot$  is  $23 \pm 2$  for X-ray luminosities  $> 3 \times 10^{37}$  ergs/s. The fact that the X-ray binary distribution is similar to that of the optical light, strongly suggests a similar formation history for single and binary stars. Latter mixing should not play a strong role, since metallicity gradients are detected in this galaxy (Kobayashi & Arimoto 1999), and otherwise would be erased.

#### 4. $\text{LOG}(N) - \text{LOG}(S)$

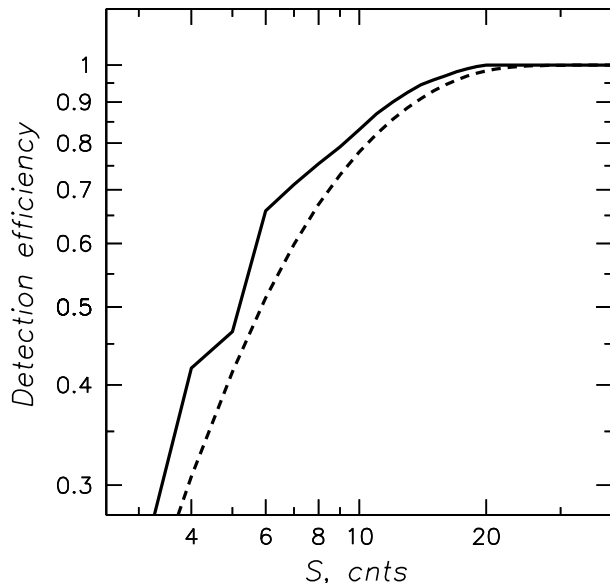


FIG. 4.— Efficiency of source detection as a function of detected counts. The solid line illustrates the decrease in the detection efficiency, seen at source counts less than 20, caused by the bright diffuse X-ray emission, changes in sensitivity (mostly due to quantum efficiency differences between the chips) and the reduced signal-to-noise due to PSF degradation at large off-axis angles. The dashed line indicates the resulting efficiency due to the Poisson migration.

In deriving the efficiency for source detection, we simulated the effect of the diffuse X-ray emission on the resulting signal-to-noise requirements for our source detection at a  $5\sigma$  statistical threshold. We also took into account the spatial distribution of sources, which are concentrated toward the center, where the 'background' is higher. This further reduces the detection sensitivity. These effects are important for source detection close to the center of M84. For sources outside the effective radius of M84, changes in the sensitivity (due primarily to quantum efficiency differences between CCD chips) and the reduced signal-to-noise, due to PSF degradation at large off-axis angles, play important roles in the detection. We estimate the resulting detection efficiency in Fig.4. The effects of strong diffuse emission are important for sources with fewer than 15 counts, while changes in the PSF affect sources with 6 counts or fewer. Because of the Poisson noise, the shape of the source luminosity distribution will be further modified (Poisson migration) and will be different for different exposure times. While a proper reconstruction requires a response matrix with the luminosity resolution defined by a Poisson process, in the present analysis, we simply correct for the amplitude of the effect, by convolving the detection efficiency with the Poisson probability distribution and show the resulting detection efficiency (which is equivalent to the completeness) in Fig.4. In the following

derivation of the  $\log(N) - \log(S)$ , we will correct for this incompleteness in the survey. Finally, changes in the sensitivity (effective area and quantum efficiency) are most important for flux correction and affect the resulting slope at high fluxes.

The resulting  $\log(N) - \log(S)$  is shown in Fig.5. In further analysis we accounted for the contribution from extragalactic sources (Giacconi et al. 2001). There is a break at the level of 19 sources (with an expected CXB contribution of 6 sources) at a corresponding luminosity of  $L_b = 4.6^{+1.2}_{-0.6} \times 10^{38}$  ergs/s (errors quoted are 68% confidence limits). The integral slope at lower fluxes is  $-0.87 \pm 0.07$ , while at higher fluxes, it is  $-1.8 \pm 0.5$ . The differential slopes at lower and higher fluxes are  $-1.79 \pm 0.18$  and  $-2.7^{+0.6}_{-1.1}$ , correspondingly. Our results for the luminosity of the break and the slope at high fluxes are in remarkable agreement with findings by Sarazin et al. (2000) for another elliptical galaxy, NGC4697, ( $L_b = 3.2^{+2.0}_{-0.8} \times 10^{38}$  ergs/s and differential slopes at lower and high fluxes of  $-1.29^{+0.49}_{-0.36}$  and  $-2.76^{+0.8}_{-2.0}$ , correspondingly). However, as we will argue below, luminosities of the break in both galaxies are derived for the averaged spectrum, which is *not typical* for NS LMXB emitting close to the Eddington.

Flattening of the source luminosity function below the luminosity of  $5 \times 10^{37}$  ergs/s, seen in NGC4697 and M31 also may be present in M84, but since we have only one point there, derived from our detection of sources with only 3 and 4 counts, it would certainly be an over-interpretation to discuss this in more detail.

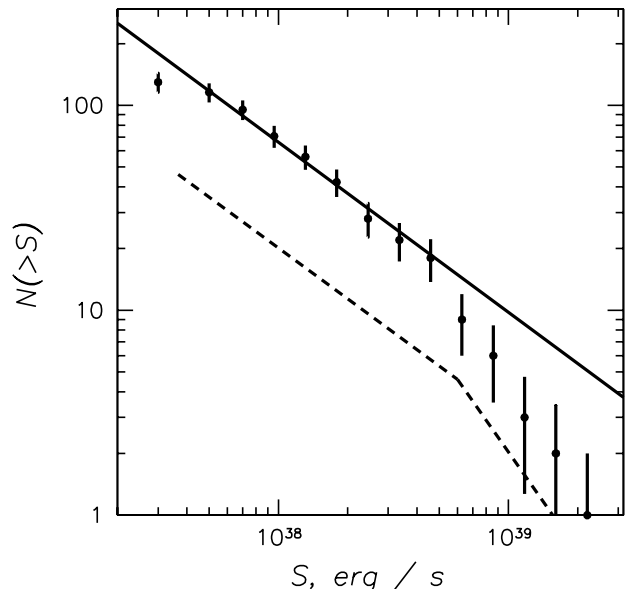


FIG. 5.—  $\log(N) - \log(S)$  of M84 sources. The dashed line indicates the CXB. Foreground sources were removed from the source list. Solid line indicates the fit to low fluxes.

#### 5. HARDNESS RATIOS

In the absence of a variation in absorption across M84, plus the lack of neutral gas in ellipticals, the source hardness ratios are particularly straightforward to interpret.

In Fig.6 we present the hardness ratios for the 32 sources with the best statistics, determined using the source counts in the Hard and Soft bands as  $(H - S)/(H + S)$ , using three independent energy bands, 0.3 – 1, 1 – 2 and 2 – 10 keV. Given the precision of the hardness ratio estimates, a

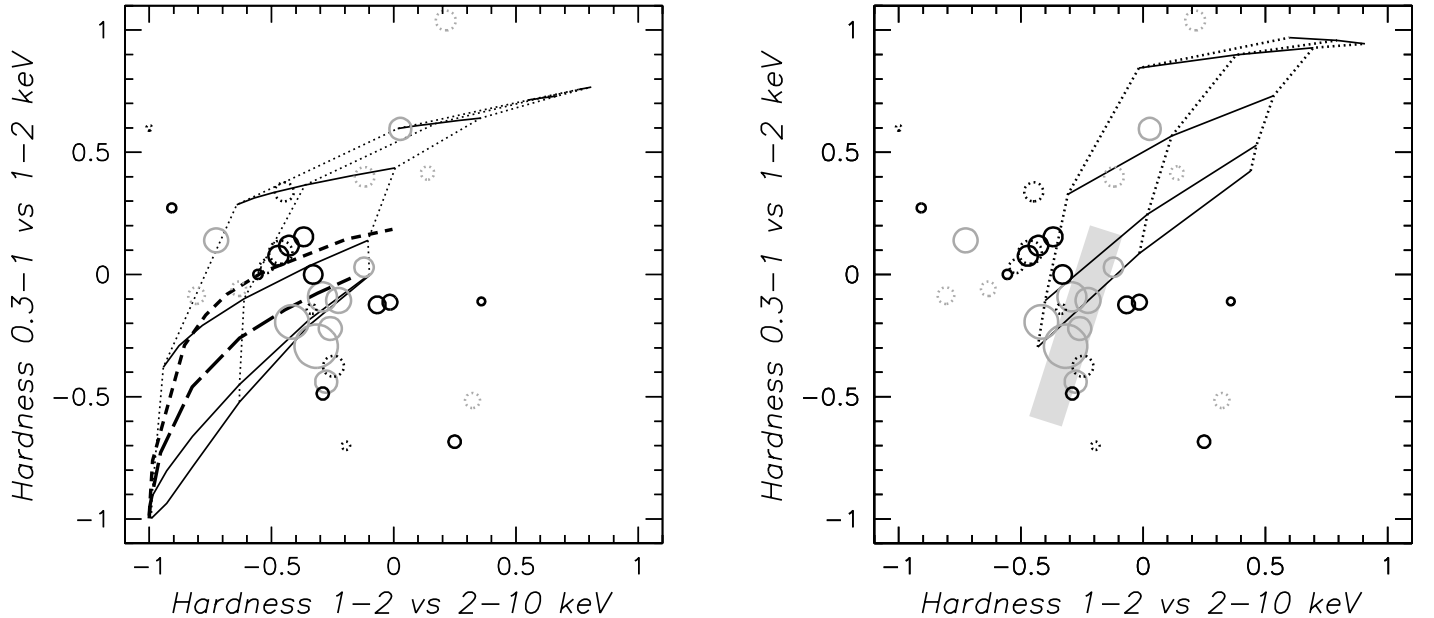


FIG. 6.— X-ray spectral diagnostic diagrams, based on source hardness ratios, determined using the background subtracted source counts in the Hard and Soft bands as  $(H - S)/(H + S)$ . Data points are shown as black circles for sources within  $2'$  of the M84 center and as grey circles otherwise. The size of the circle is proportional to the logarithm of the flux and circles are drawn with a solid line when the uncertainty in the hardness ratio estimation is less than 0.1, with a dotted line for uncertainties less than 0.2. The differences between the *left* and *right* panels are only in the model grids. On the *left* the long-dashed line denotes a hardness ratio from the bremsstrahlung model, the short-dashed line corresponds to the model of a multicolor black-body disk by Makishima et al. (1986). We also plot a grid corresponding to a comptonized 10 keV plasma black-body spectrum with a blackbody temperature of 0.01, 0.1, 0.2, 0.4, 0.8, 1.6, 3 keV (the solid lines) and optical depth for comptonization of 0.1, 1.6, 6.4 (the dotted lines). In the *right* panel the shaded area denotes the loci for type-1 AGN. A grid illustrates the hardness ratios for power law models with photon indices  $\Gamma = 0, 1, 2$  (dotted lines) and neutral hydrogen absorption (in the observed frame) of  $\log(nH) = 20.5, 21, 21.5, 22, 22.5$  (solid lines), typical for the hard background sources found by XMM (Hasinger et al. 2001).

combination of first vs second (HR21), and second vs third (HR32) reveals the largest spread in the points and therefore provides better tests for the predictions from various spectral models.

We subdivide the source sample into two parts, within or outside two effective radii, as we expect almost no background sources to be detected in a small region close to the center of the galaxy. The larger number of sources available at larger radii, allows us to better sample the X-ray colors. The  $\log(N) - \log(S)$  of M84 sources and of cosmic X-ray background sources are quite similar in the observed flux range. In the whole field used for source detection, CXB sources constitute almost 1/3 of the detected sources, i.e. in Fig.6, 11 background sources should appear, including 6 of high statistical significance (solid circles). Given the energy band of Chandra and using the results of point source hardness ratios and  $\log(N) - \log(S)$  analysis from the deep XMM pointing of the Lockman hole (Hasinger et al. 2001), we conclude that 1/3 of the background sources should exhibit hard colors (within the power law - nH grid shown in Fig.6, note that a variation of nH is intrinsic to AGN), while the other 2/3's should be within the grey-shaded area on the right panel of Fig.6 of ROSAT-type background sources (type 1 AGN). In fact a fraction of the ROSAT-type background sources should be larger, due to differences in the sensitivity between Chandra and XMM at high energies.

We find two concentrations of hardness ratios. The first (black circles in Fig.6) corresponds to that expected for a multicolor disk black-body model (Makishima et al. 1986; *diskbb* model in XSPEC) with a central black-body tem-

perature near 0.5 keV. The second (gray circles in the shaded area on the right panel of Fig.6) corresponds to power law indices between 1 and 2. The empirical relation between the luminosity and the spectral shape, derived for the Milky Way sources, implies that luminous high state LMXB's should be dominated by a thermal component, while for sources in the low state, the spectrum is harder. This is in a good agreement with our detection of a number of sources with thermal disk emission, which includes most of the sources with flux levels near the break in the luminosity function. Thus, although the disk black-body model cannot account for all the observed X-ray colors, the large concentration of M84 sources about the prediction of this model allows us to distinguish them from CXB sources. Among the remaining sources there are four that follow the prediction of the black-body spectrum (the furthest to the left dotted line in the comptonization grid in the left panel of Fig.6). Their luminosities exceed the Eddington limit for a neutron star. Other sources exhibit both a soft-excess and a hard tail (these sources fall in the lower right of the diagram). The hard tail in M84 sources could be produced by comptonization on the hot plasma ( $kT \sim 10$  keV) with typical  $\tau = 1 - 3$  and a soft input spectrum  $kT < 0.1$  keV (Sunyaev & Titarchuk 1985; Titarchuk 1994; *comptt* model in XSPEC).

Our conclusions regarding the origin of X-ray colors in M84 LMXBs are in agreement with a much more developed scheme for X-ray binaries in the Galaxy (e.g. Done 2002). The next step would be then to employ the luminosity-spectrum relation, established for the Milky Way sources to separate the NSs from BHs in M84 at low

luminosities. Given that the luminosities of M84 sources with well measured colors exceed  $10^{38}$  ergs/s, the soft component should still be dominant in LMXBs with a black-hole primary, yet their Milky Way prototypes exhibit a large spread in colors. On the other hand, the majority of LMXBs with NS-primary should be Z-sources (like Cyg X-2), that are characterized by a modest variation in colors. Following these guidelines, X-ray black holes comprise up to 1/3-1/2 of the X-ray sources in M84. Chandra observations of the Sombrero galaxy (Delain et al. 2002), indicates a somewhat smaller, yet similar fraction of accreting black holes (1/4). While small-number statistics prevents us from a firm conclusion, the observed differences are in line with the suggestion of a gradual built-up of black-holes in the 1.5-3  $M_{\odot}$  range (Prokhorov & Postnov 2001).

## 6. DISCUSSION

### 6.1. *The break: Eddington limit on isotropic radiation from accretion of matter on the neutron star.*

We note in §5, that sources near the break of the luminosity function have similar spectra. Their spectra are softer than the average one. Therefore, using a softer spectrum we find the break in the luminosity function occurs at  $L_b = 2.4_{-0.3}^{+0.6} \times 10^{38}$  ergs/s (a factor 0.52 lower than the estimate using the averaged spectrum). The Eddington limit also should be corrected for the  $\mu_p = \langle A \rangle / \langle Z \rangle$ , which for the typical solar metallicity of stars in M84 is 1.17. Thus the corrected value for the isotropic emission from accretion of matter of solar elemental composition onto a neutron star is  $2.1 \times 10^{38}$  ergs/s, which agrees well with our measurements of the break.

The existence of a limiting luminosity arising from accretion onto a neutron star has been debated by several authors. Paczyński & Wiita (1980) proposed that at supercritical accretion rates, the resulting luminosity could be much higher than the Eddington luminosity. Thus, our result of a very close match between the break luminosity and the Eddington luminosity is important in modeling the structure of the inner accretion zone. Inogamov & Sunyaev (1999) find that at accretion rates close to critical, emission from the surface of the neutron star becomes softer, comparable to the emission from the disk. Compared to emission from the disk, spectrally harder emission from the surface of the neutron star is expected at lower accretion rates and together with black holes is probably responsible for the harder colors of the combined spectrum.

A prediction of a cut-off in the luminosity function is not unique to the Eddington limit. For example, on a basis of LMXB evolution, Wu (2001) predicts a gradual decrease in the number of accreting systems with high mass transfer rates with galactic age, with a luminosity function exhibiting an exponential cut-off. However, a close correspondence of the break in the luminosity function to the Eddington luminosity, also seen in star-forming galaxies (Körding, Falcke, Markoff 2002), is a strong argument in favor of the relation of the break to the limiting luminosity.

### 6.2. *The high end of the luminosity function: the mass function of accreting black holes*

Chandra observation of M84 reveal 5 to 10 sources (the number is sensitive to the behavior of the luminosity function just above the break), whose luminosity exceeds the Eddington limit for accretion onto a neutron star. When BH LMXBs (LMXBs with a black hole primary) are used to explain the high-luminosity end of the source population in M84, a problem arises in explaining why such a steep dependence of source number on luminosity becomes flatter below  $\sim 2 \times 10^{38}$  ergs/s. One can seek an explanation in terms of the specific BH LMXB luminosity function<sup>1</sup>, but such a coincidence with the Eddington limit is unlikely. On the other hand, it is natural to attribute this to the black-hole mass-function. In this case, the differential slope of the black hole luminosity function should be shallower than -1.79, or no break would be seen, while a steeper slope of the luminosity function above the break is a result of convolution of the black hole mass and luminosity functions. Using our measurements, we can constrain the differential slope  $\alpha$  of the mass function for accreting black holes in M84 to be  $-2.7 < \alpha < -0.9$ , where the lower limit comes from an assumption that black holes shine at their Eddington limit and the upper limit corresponds to similar luminosity functions of LMXBs with black-hole and neutron star primaries. The statistical significance of the slopes quoted above is the same as for the slope at high luminosities ( $_{-2.0}^{+0.8}$ ).

Besides accreting black holes, explanations for the appearance of super-Eddington sources, based on an accreting neutron star could be: beaming of the radiation, flaring and super-Eddington accretion rates. Each of these scenarios has difficulties explaining the observed luminosity function of M84. Observational examples of super-Eddington accretion rates, such as for SS433, demonstrate that the luminosity does not exceed the Eddington limit by more than a factor of two. Occurrence of a break in the observed luminosity function at the Eddington limit for *isotropic* radiation would be hard to reproduce in the beaming scenarios. As the existence of stellar mass black-holes is not disputed, our conclusion on the effect of black-hole mass function provides most likely explanation for the observed behavior of the M84 source luminosity function at high fluxes.

The brightest candidate galactic source in M84 has a luminosity of  $1.6 \times 10^{39}$  ergs/s. In the inner 2' region of M84, where most of the galactic sources should be located and where the CXB contamination is low, the brightest source has a luminosity of  $0.9 \times 10^{39}$  ergs/s. This is contrary to the very luminous sources found in the Antennae galaxies and other star-forming galaxies, whose spectral characteristics also are different (Fabbiano, Zezas, Murray 2001; Makishima et al. 2000). Interpretation of the Antennae sources could be either via beaming (King et al. 2001; Körding, Falcke, Markoff 2002; Zezas & Fabbiano 2002) or exceeding the Eddington limits (Begelman 2002).

### 6.3. *Low end of the luminosity function: sampling the initial distribution of binaries with NS primaries*

To relate the observed luminosity function to the distribution of objects with different physical parameters, we need to make an assumption about the origin of the accre-

<sup>1</sup>We define the specific luminosity function, as a distribution of luminosities (resulting from a distribution of the accretion rates) for a *given* mass black hole.

tion process. Two major scenarios are possible, accretion from a main sequence star or accretion caused by nuclear evolution of the secondary.

The first scenario dominates for LMXBs in the Milky Way and can accommodate both the high accretion rates and short periods of the LMXB systems. To apply this model to the observed luminosity function of LMXBs in M84, we need to consider systems with relatively high accretion rates (typically in excess of  $10^{-9} M_{\odot} \text{ yr}^{-1}$ ). At these accretion rates, assuming they are persistent, observed LMXBs must have formed recently (less than a Gyr ago). The old age of the stellar population (12 Gyr) implies that the fraction of active systems is  $1/100$ – $1/10$  of the integral LMXB production (a factor of  $\Delta T/T$ ). Yet, as the time since star formation increases, different mechanisms come into play. However, for accretion from a main sequence star, magnetic braking (Verbunt & Zwaan 1981) can change the behavior of period over time. For example, for a similar mass range, which we take as  $0.3 - 1 M_{\odot}$  for the secondary, and using the prescription for the magnetic braking from Wu (2001), at 12 Gyr after star-formation, binaries with longer initial periods (0.3-1.3 days) are important, compared to those with periods shorter than 0.3 days that dominate the accretion process only 0.1 Gyr after star-formation. Therefore, the LMXB population in galaxies of different ages essentially samples different parts of the initial period distribution. The effect should be seen in comparison studies between galaxies and will provide clues to binary formation (Kalogera & Webbink 1998).

For LMXBs with an evolved secondary, the luminosity and period of the system are not independent. Assuming a 20% efficiency for accretion, the luminosity of LMXBs is given by  $0.4 \times 10^{37} P_d^{0.93} M_2^{1.47}$  ergs/s for accretion from an evolved companion, where  $P_d$  and  $M_2$  are the period of the binary in days and mass of the secondary in  $M_{\odot}$  (Webbink et al. 1983). Given the typical solar mass for the secondary, the luminosity of  $10^{38}$  ergs/s requires periods on the order of ten days. Most LMXBs in the Milky Way have short periods, but the Milky Way star-formation also could be recent (note that the observational appearance of LMXBs in the Milky Way bulge is generally attributed to high kick velocities, *e.g.* White & Ghosh 1998). While studies

of periodicities of LMXBs in ellipticals are the most direct way to disentangle systems with evolved secondaries from those with main sequence secondaries, the required collecting area for such observations will only be available with new generations of X-ray telescopes (*e.g.* XEUS). Element composition of the accreting material from an evolved secondary is dominated by helium. This increases the Eddington limit by a factor of two. Therefore, observing a lower value for the Eddington limit, favors accretion from main sequence stars in LMXBs.

Finally, we would like to comment on the production of LMXBs in globular clusters. Stellar trapping by a compact object in globular clusters can lead to LMXB formation (Kuranov, Postnov, Prokhorov 2001). Although the number of X-ray sources associated with globulars exceeds the average expected for their light, the number is still a small fraction of the total number of sources ( $\sim 10\%$ ) in some ellipticals (Sarazin et al. 2000; Kraft et al. 2001). Therefore, if globulars are a primary site for LMXB production in early-type galaxies, to explain the LMXBs outside globular clusters either globular clusters have been disrupted or a “kick” expelled the LMXB (as during the collapse of the white dwarf into the neutron star). Indirectly the importance of globulars can be estimated by comparative studies (White 2001). In addition, the outskirts of brightest cluster galaxies, for example NGC1399 and M87, are characterized by an astonishingly high frequency of globulars, which explains a strong association of globulars with X-ray sources in the *outskirts* of NGC1399 found by Angelini, Loewenstein, Mushotzky (2001).

#### ACKNOWLEDGMENTS

This work was supported by NASA grants GO0-1045X and AG5-3064 and the Smithsonian Institution. AF has benefited from discussions with Andrei Beloborodov, Eugene Churazov, Guenther Hasinger, Vicky Kalogera, Wolfgang Pietsch, Konstantin Postnov, Juri Poutanen, Sergey Sazonov, Rodrigo Supper, Yasuo Tanaka and Andreas Zezas at various stages of the presented research. AF acknowledges receiving the Max-Planck-Gesellschaft Fellowship. Authors thank the referee for useful comments on the manuscript.

#### REFERENCES

- Angelini, L., Loewenstein, M., Mushotzky, R.F. 2001, ApJ, 555, L21  
 Bailyn, C.D., Jain, R.K., Coppi, P., Orosz, J.A. 1998, ApJ, 499, 367  
 Begelman, M.C. 2002, ApJ accepted, (also astro-ph/0203030)  
 Done, C. 2002, preprint astro-ph/0203246  
 Delain, K., Forman, W., Jones, C., Murray, S., Kraft, R. 2002, AAS meeting  
 Fabbiano G., Zezas A., Murray S.S. 2001, ApJ, 554, 1035  
 Finoguenov, A., and Jones, C. 2001, ApJ, 547, 107  
 Fryer, C.L. & Kalogera, V. 2001, ApJ, 556, 340  
 Giacconi, R., Gursky, H., Paolini, F.R., Rossi, B. 1962, Phys. Rev. Let., 9, 439  
 Giacconi, R., Rosati, P., Tozzi, P., Nonino, M., Hasinger, G. et al. 2001, ApJ, 551, 624  
 Hasinger, G., et al. 2001, A&A, 365, 45  
 Iben, I. Jr., Tutukov, A.V., Yungelson, L.R. 1995, ApJS, 100, 217  
 Inogamov, N.A., Sunyaev, R.A. 1999, AstL, 25, 269  
 Kahabka, P., and van der Heuvel, E.P.J. 1997, ARA&A, 35, 69  
 Kalogera, V., Kolb, U., King, A.R. 1998, 504, 967  
 Kalogera, V., Webbink, R.F. 1998, ApJ, 493, 351  
 King A.R., Davies M.B., Ward M.J., Fabbiano G., Elvis M., 2001, ApJ, 552, L109  
 Kobayashi C., Arimoto N., 1999, ApJ, 527, 573  
 K rding, E., Falcke, H., Markoff, S. 2002, A&A, 382, L13  
 Kraft, R.P., Kregenow, J.M., Forman, W.R., Jones, C., Murray, S.S. 2001, ApJ, 560, 675  
 Kuranov, A.G., Postnov, K.A., Prokhorov, M.E. 2001, ARep, 45, 620  
 Makishima, K., Maejima, Y., Mitsuda, K., Bradt, H.V., Remillard, R.A., Tuohy, I.R., Hoshi, R., Nakagawa, M. 1986, ApJ, 308, 635  
 Makishima, K., Kubota, A., Mizuno T., et al. 2000, ApJ, 535, 632  
 Paczyński, B. 1967, Acta Astron., 17, 287  
 Paczyński, B., and Wiita, P.J. 1980, A&A, 88, 23  
 Prokhorov, M.E., Postnov, K.A. 2001, ARep, 45, 899 (also astro-ph/0110176)  
 Sarazin, C.L., Irwin, J.A., Bregman, J.N. 2000, ApJ, 544L, 101  
 Schweizer, F., and Seitzer, P. 1992, AJ, 104, 1039  
 Sunyaev, R. & Titarchuk, L. 1985, A&A, 143, 374  
 Tanaka, Y. & Shibazaki, N. 1996, ARAA, 34, 607  
 Titarchuk, L. 1994, ApJ, 434, 570  
 Verbunt, F., and Zwaan, C. 1981, 100, L7  
 Vikhlinin, A., Forman W. 1995, 455L, 109  
 Vikhlinin, A., Forman, W., Jones, C., Murray, S. 1995, ApJ, 451, 542  
 Webbink, R.F., Rappaport, S., Savonije, G.J. 1983, ApJ, 270, 678  
 White, N.E., Ghosh, P. 1998, ApJ, 504, 31  
 White, R.E. III 2001, preprint astro-ph/0111293  
 Worthey, G. 1994, ApJS, 95, 107  
 Wu, K. 2001, preprint astro-ph/0103157  
 Zezas, A., Fabbiano, G. 2002, ApJ submitted (astro-ph/0203176)